发光学报
CHINESE JOURNAL OF LUMINESCENCE
中文核心期刊
主管：中国科学院
主办：中国科学院长春光学精密机械与物理研究所
中国物理学会发光分会
主编：申德振

基于新型复合传输层的有机太阳能电池模组器件

丁磊，佛婉贞，董豪杰

引用本文:
丁磊, 佛婉贞, 董豪杰. 基于新型复合传输层的有机太阳能电池模组器件[J]. 发光学报, 2021, 42(2): 231-240.
DING Lei, FO Wan-zhen, DONG Hao-jie. Organic Solar Cell Module Device Based on A Novel Composite Transport Layer[J]. *Chinese Journal of Luminescence*, 2021, 42(2): 231-240.

在线阅读 View online: https://doi.org/10.37188/CJL.20200344

Article ID: 1000-7032(2021)02-0231-10

Organic Solar Cell Module Device Based on A Novel Composite Transport Layer

DING Lei[1,2*], FO Wan-zhen[1], DONG Hao-jie[1]

(1. *School of Electrical Information and Artificial Intelligence, Shaanxi University of Science and Technology, Xi'an* 710021, *China*;
2. *Jiangsu Jitri Org Optoelectronics Technology Co., Ltd., Suzhou* 215215, *China*)

* *Corresponding Author, E-mail: dinglei@sust.edu.cn*

Abstract: Based on a new composite interface transport layer, large-area organic solar cell module was fabricated by vacuum evaporation of organic small molecular materials. According to the transmittance spectrum, surface roughness morphology and surface wettability of transport layer, the surface roughness of active layers based on different substrates, the uniformity of blade coating and the influence of different transport layers on the performance of organic solar cells were analyzed. The experimental results show that when the electronic dense layer of 4,7-diphenyl-1,10-phenanthroline(BPhen) acetylimide is deposited on the surface of aluminum-doped zinc oxide substrate, the new composite transport layer is formed, which does not affect the light transmittance of the substrate in the range of 300 – 900 nm. In addition, the electron dense layer of BPhen can effectively improve the flatness and wettability of the substrate surface, which is beneficial to the subsequent scraping of the active layer solution and improves the quality and the stability of the coating film. By analyzing the surface roughness and three-dimensional morphology of the active layer film coated on different substrates, the surface roughness of the active layer film coated on the AZO(Al doped ZnO)/BPhen new composite transport layer was significantly reduced. It means that the new composite transport layer as substrate is beneficial to scrape out a uniform active layer film. As a result, the open circuit voltage(V_{oc}), short-circuit current density(J_{sc}) and fill factor(FF) of rigid and flexible module device are significantly improved, and the power conversion efficiency(PCE) of the new rigid modular device is increased to 10.62%, which is about 13% higher than stand device. Importantly, the PCE of the flexible module device reaches 5.13%, which is also approximately 32% higher than AZO-based device.

Key words: new composite transport layer; organic solar cell module; electron dense layer
CLC number: TM914.4 **Document code**: A **DOI**: 10.37188/CJL.20200344

基于新型复合传输层的有机太阳能电池模组器件

丁 磊[1,2*], 佛婉贞[1], 董豪杰[1]

(1. 陕西科技大学 电子信息与人工智能学院, 陕西 西安 710021; 2. 江苏集萃有机光电技术研究所有限公司, 江苏 苏州 215215)

摘要: 通过刮涂制备薄膜衬底和真空蒸镀有机小分子材料来构筑复合界面传输层,制备了大面积有机太阳

收稿日期: 2020-11-10; **修订日期**: 2020-12-15
基金项目: 国家自然科学基金(22005184); 陕西省科技计划项目创新计划(2011KTCQ01-09); 陕西省重点研究发展计划(2017ZDCXL-GY-06-03); 陕西省教育厅特殊科研计划(17JK0095); 江苏省青年基金会项目(BK20180288); 第六十二期中国博士后科学基金(713170091)资助项目
Supported by National Natural Science Foundation of China(22005184); Innovation Project of Science and Technology Plan Projects of Shaanxi Province(2011KTCQ01-09); Key Research and Development Plan of Shaanxi Province(2017ZDCXL-GY-06-03); Special Scientific Research Plan of Shaanxi Provincial Education Department(17JK0095); Jiangsu Youth Foundation Project(BK20180288); Sixty-second Grants from China Post-doctoral Science Fund(713170091)

能电池模组器件。通过透射光谱、传输层粗糙度形貌、表面浸润性、不同衬底的光吸收层粗糙度形貌、刮涂的均匀性研究了同传输层对 OSCs 器件性能的影响。实验结果表明,当在 AZO 衬底表面蒸镀一层电子致密层时,即新型复合传输层并未影响基片在 300 ~ 900 nm 范围内的透过率,并且 BPhen 电子致密层可以有效地提高基片表面的平整度和浸润性,这也有利于后续光吸收层溶液的刮涂,提高涂膜的质量和稳定性。通过不同基底刮涂光吸收层薄膜表面粗糙度以及形貌图,其新型复合传输层作为衬底刮涂出的光吸收层薄膜的表面粗糙度有了明显的降低,表明平整的基底有利于刮涂出表面均一的薄膜。由此制备的基于新型复合传输层的刚性、柔性模组器件的开路电压(V_{oc})、短路电流密度(J_{sc})和填充因子(FF)都有大幅度的提高。最终制备的新型刚性模组器件光电转化效率(PCE)提高到 10.62%,提升了约 13%;柔性模组器件的光电转化效率(PCE)达到 5.13%,提升了 32%。

关 键 词:新型复合传输层;有机太阳能电池模组;电子致密层

1 Introduction

Organic solar cells (OSCs) have attracted a wide attention due to their advantages of low cost, large area manufacturing, flexibility and environmental friendliness[1-6]. At present, organic solar cells are developing rapidly, in the laboratory stage their photoelectric conversion efficiency (PCE) has exceeded 17%[7-17]. Therefore, it is urgent to carry out relevant industrial studies, which is necessary for the preparation of high-efficiency organic solar cell module devices[18-23]. Therefore, organic solar cell modules prepared by doctor-blade coating (DBC) should have good repeatability and maintain excellent conversion efficiency. The film forming property, uniformity and stability of the active film will be affected by the surface morphology of the different transport layer substrate. In the process of large-area scraping and coating, the differences of film thickness in different areas, and bad surface morphology and blending state of active layer will lead to the attenuation of module device performance[24-28]. At the same time, an interface transport layer with excellent performance can greatly restrain intrinsic defects and interfacial defects, improve the efficiency of carrier collection, and improve the PCE of module devices, which has the potential to promote the industrialization of organic solar cells.

Thus, this research proposes a new type of composite transport layer based on AZO/BPhen small molecule materials, which was constructed by vacuum evaporation of BPhen on the surface of the blade coated AZO film. The method of combining blade coating and vacuum evaporation can realize the hole filling and defect passivation of AZO film, which can improve the carrier collection efficiency and the surface smoothness. Therefore, the stability and PCE of organic solar cell module were effectively improved. In addition, this method is suitable for the preparation of flexible organic solar cells with highly repeatability.

2 Materials and Methods

2.1 Materials

Indium tin oxide (ITO) glass was purchased from South China Xiang Science and Technology Company, Ltd.. AZO is Al doped ZnO[29]. Zincacetate dihydrate ($Zn(CH_3COO)_2 \cdot 2H_2O$, 98%) were purchased from Sigma-Aldrich. Aluminum nitrate ($Al(NO_3)_3 \cdot 9H_2O$, 99.99%) was purchased from Aladdin. BPhen was purchased from Shaanxi Lighte Optoelectronics Material. Chloroform (99.8%) was purchased from damas-beta. For the active layer, the mixture of Poly[(2,6-(4,8-bis(5-(2-ethylhexyl-3-fluoro) thiophen-2-yl)-benzo[1,2-b:4,5-b′] dithiophene))-alt-(5,5-(1′,3′-di-2-thienyl-5′,7′-bis(2-ethylhexyl) benzo[1′,2′-c:4′,5′-c′] dithiophene-4,8-dione)] (PM6):(2,2′-((2Z,2′Z)-(12,13-bis(2-ethylhexyl)-3,9-diundecyl-12,13-dihydro-[1,2,5] thiadiazolo[3,4-e] thieno [2″,3″:4′,5′] thieno [2′,3′:4,5] pyrrolo [3,2-g] thieno [2′,3′:4,5] thieno [3,2-b] indole-2,10-diyl) bis (methanylylidene)) bis (5,6-difluoro-3-oxo-2,3-dihydro-1H-indene-2,1-diylidene)) dimalononitrile) (Y6) at a weight ratio of 1:1.2 with a concentration of 18 mg/mL was dissolved in Chloroform (CF).

1-Chloronaphthalene(CN) was added to the CF at various concentrations of 1.5%.

2.2 Device Fabrication

As shown in Fig. 1(a), it is a schematic diagram of the device structure of traditional OSCs. The structure of OSCs is ITO/AZO(20 nm)/PM6∶Y6(100 nm)/MoO_3(10 nm)/Al(300 nm).

Fig. 1(b) is a schematic diagram of the device structure of the new composite transport layer OSCs. The structure of OSCs is ITO/AZO(20 nm)/4,7-Diphenyl-1,10-phenanthroline (BPhen) (10 nm) PM6∶Y6(100 nm)/MoO_3(10 nm)/Al(300 nm). Fig. 1(c) shows the chemical structure of the material used in the device. The preparation process of the new composite transport layer OSCs device is as follows: (1) Glass substrate was polished first, and then an ITO film was plated on the glass by magnetron sputtering to form ITO conductive glass as the cathode of the solar cell. (2) Patterned laser etched ITO conductive glass. (3) AZO solution was scraped on the patterned ITO conductive glass (The slit height was 20 μm[23]. The substrate temperature was 40 ℃, and the scraping rate was 30 mm/s.). The film was obtained by annealing at 140 ℃ for 20 min in the air. (4) ITO coated with AZO film was placed in the nitrogen gloves box inside of the vacuum coating machine. When the cabin pressure was pumped to 3×10^{-4} Pa, BPhen organic small molecular material of 10 nm was steam plated at a rate of 0.2 nm/s to construct the composite transport layer. (5) Take out the evaporated substrate and place it on the scraper in the air for scraping and painting the light absorption layer solution. The active layer solution is a binary system solution divided into two groups PM6 and Y6, with a ratio of PM6∶Y6 = 1∶1.2. (6) Stir all solutions for 6 h before used (The height of the slit is 20 μm, the substrate temperature is 60 ℃, and the scraping speed is 40 mm/s.). Then anneal at 110 ℃ for 10 min resulted in a light absorption film thickness of 100 nm. (7) The battery sheet scraped and coated with the light absorption film was placed in the vacuum evaporation machine. When the cabin pressure was pumped to 3×10^{-4} Pa, 10 nm thickness of MoO_3 was evaporated as the cavity transport layer at 0.01 nm/s evaporation rate. (8) Take out the battery slice and put it into a mold for physical partition. 1 mm electrode is exposed for connecting the top and the bottom between modules to build the batteries connected in series. Then put the battery slice in the coating machine, evaporate the 300 nm aluminum electrodes at the evaporation rate of 0.1 nm/s after the cabin pressure is pumped

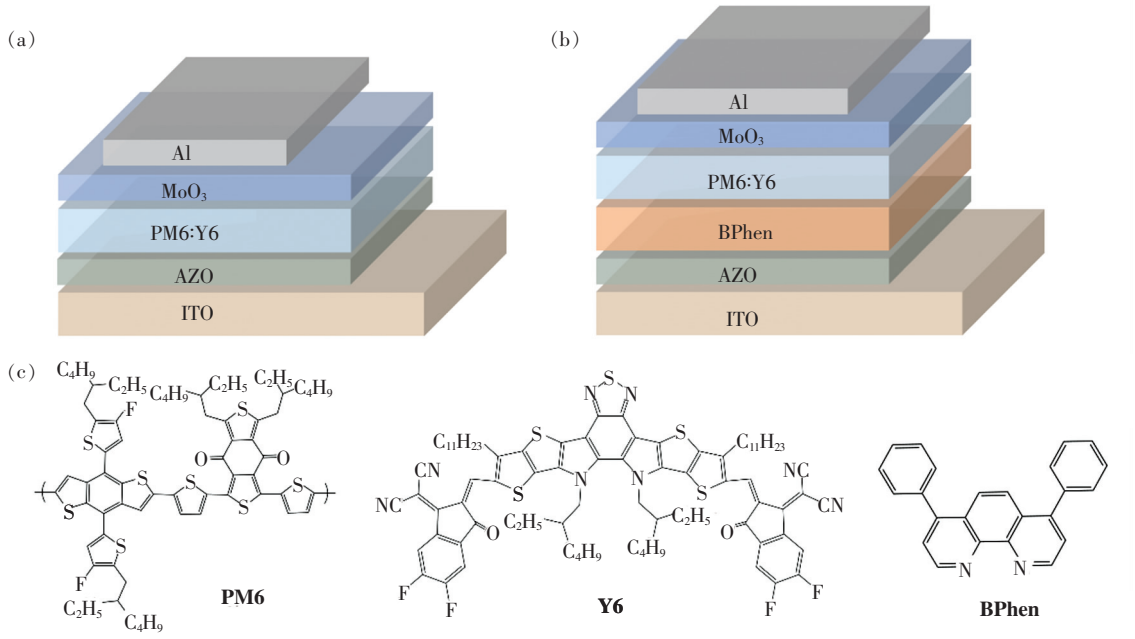

Fig. 1　(a) – (b) Schematic diagrams of the device structure of traditional OSCs and the new composite transport layer. (c) Chemical structure of the material used in the device.

to 3×10^{-4} Pa.

Fig. 2(a) and (c) show the design drawings of large-area OSCs, which comprising 12 cells connected in series. Each cell is 0.4 cm in width and 7.5 cm in length and the intervals is 0.1 cm. The total active area of a large-area OSC is 36 cm^2. The output voltage could be controlled by dominant the amount of cells in series. The cathode of each cell is connected to the ITO of adjacent right-side cell for series connection. However, in the batteries connected in series, every cell must be good running to make sure the circuit is connected. Therefore, how to control the uniformity of film is important. Fig. 2(c) and (d) show the metal mask used to define the active layer by mechanical scratch for the series connection amongst the cells. Fig. 2(e) shows the blade coating process, which first uses a pipette to deposit solution and then spreads of solution through capillary action.

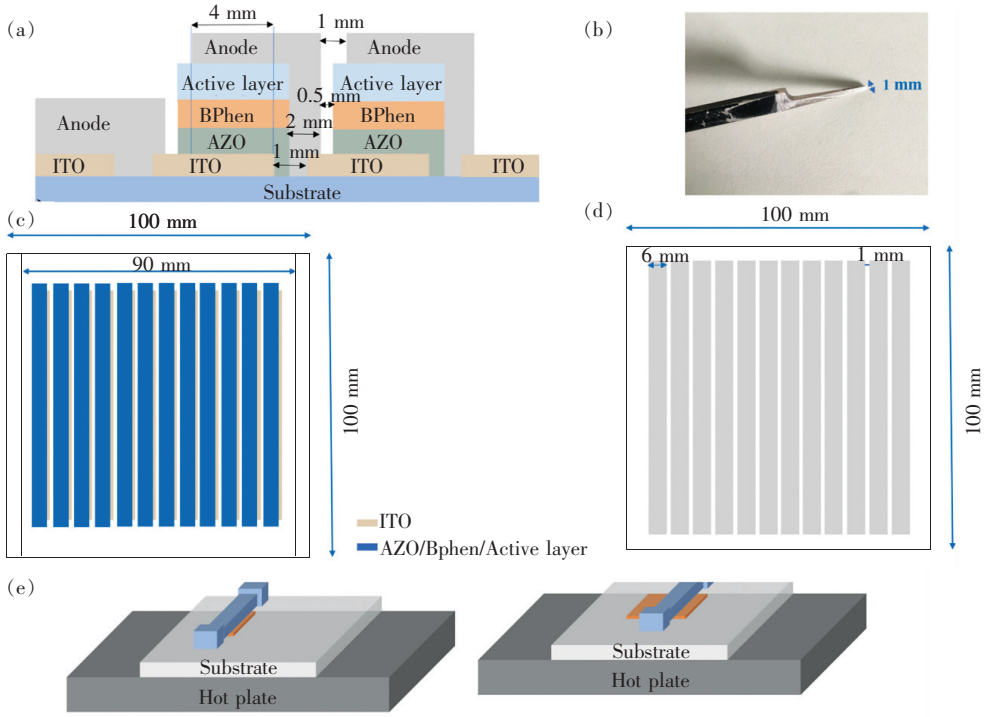

Fig. 2 Design of large-scale patterned OPV in series with side view(a) and top view(c). (b) Photo of the knife's edge. (d) A metal mask for active region definition and interconnection. (e) Blade coating process.

3 Results and Discussion

3.1 Physical Characteristics of Different Transport Layers

In order to study the influence of different transport layers on the performance of OSC devices, we prepared traditional transport layer AZO films and new composite transport layer AZO/BPhen films on glass substrates. Fig. 3 shows the transmittance curves of the glass substrate/AZO and glass substrate/AZO/BPhen structures. It can be seen from the curve that when an electron dense layer is deposited on the AZO substrate surface, and it has no effect on the transmittance of the substrate in the range of 300 – 900 nm, which ensures that the overall performance of the module device was not be affected.

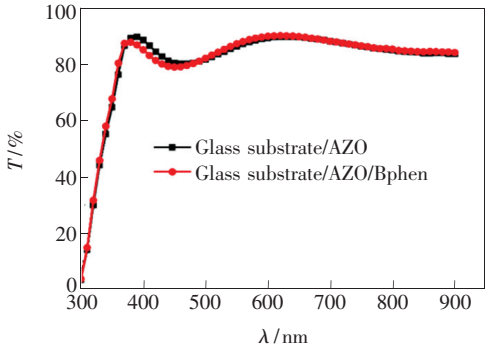

Fig. 3 Transmittance curves of glass substrate/AZO and glass substrate/AZO/BPhen structures

Because the surface morphology of the transport layer substrate is different, the film forming property, uniformity and stability of the next layer of film

prepared by scraping and coating will be further affected. So we prepared different transport layers with different morphologies for test. Fig. 4 shows the roughness of the surface of the glass substrate/AZO and glass substrate/AZO/BPhen structure with two-dimensional view.

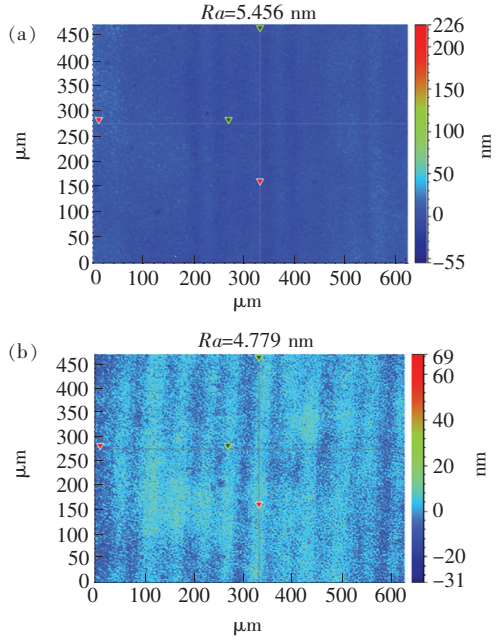

Fig. 4　Two-dimensional plan view of surface roughness of glass substrate/AZO (a) and glass substrate/AZO/BPhen (b) structure

The arithmetic mean difference (Ra) of the active layer is reduced from 5.456 nm to 4.779 nm under different substrates (the glass substrate/AZO and glass substrate/AZO/BPhen structure).

From the figure we could recognize that when an electron dense layer (BPhen layer) is deposited on the electron transport layer (BPhen layer and AZO layer), the surface roughness effectively reduced, which is benefited to the increasing of stability and uniformity of subsequent active layer coating.

Fig. 5 shows the three-dimensional surface morphologies of the glass substrate/AZO and glass substrate/AZO/BPhen structures. As shown in Fig. 5, the glass substrate/AZO has a drastic fluctuation of the thickness, which indicates that the entire surface is not flat enough. By adding an electron dense layer, we can effectively fill the holes defects of the AZO substrate, which make the entire base surface more flat, and significantly impact the quality of the subsequent coating film.

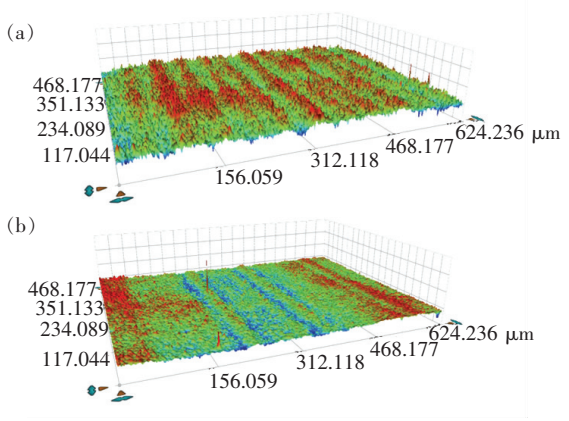

Fig. 5　Three-dimensional surface morphologies of glass substrate/AZO (a) and glass substrate/AZO/BPhen (b) structure

Then, we studied the difference of the surface wettability of different transport layers through measuring the contact angles. As shown in Fig. 6, the contact angle (θ) of chloroform solution changed from 43.1° to 41.2° for the glass substrate/AZO and glass substrate/AZO/BPhen structure. It can be found that when the electronic dense layer of BPhen is added to the AZO surface, it can effectively improve

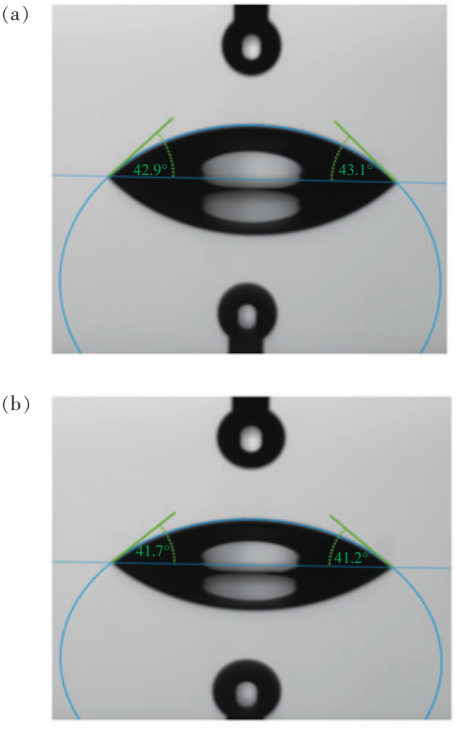

Fig. 6　Contact angle test diagrams of glass substrate/AZO (a) and glass substrate/AZO/BPhen (b) structure

the flatness and wettability of the substrate surface, which is also benefited to the subsequent knife coating process of the light absorption layer solution, thus improves the quality and stability of the coating film.

3.2 Characteristics of Active Layer Based on Different Transport Layer Substrates

An excellent interface transport layer can greatly reduce the intrinsic defects and interface defects, further improved the carrier collection efficiency and the photoelectric conversion efficiency of the module device. For this reason, we studied the surface roughness and morphologies of the active layer based on different transport layer substrates. As shown in Fig. 7, when an electron dense layer is added to the electron transport layer, the surface roughness of the active layer scraped as a substrate has been significantly reduced. The *Ra* of the active layer is reduced from 6.452 nm to 5.887 nm for glass substrate/AZO and glass substrate/AZO/BPhen structure. This indicates that a flat base is beneficial to scraping a uniform surface film.

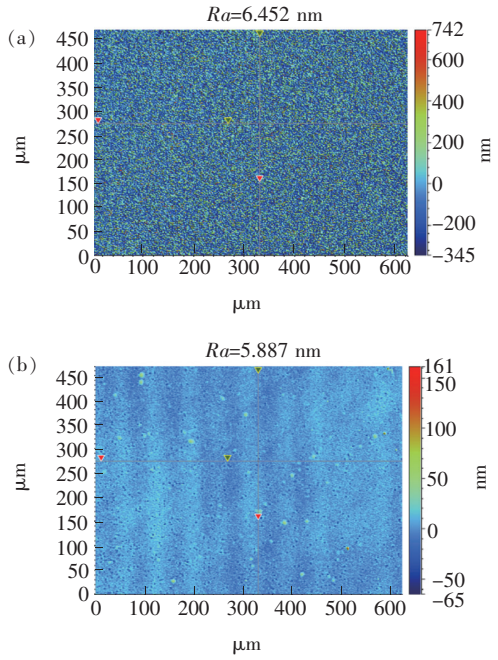

Fig. 7 Two-dimensional plan view of the surface roughness of the active layer based on glass substrate/AZO/active layer(a) and glass substrate/AZO/BPhen/active layer (b) structure

Fig. 8 shows the three-dimensional surface morphology of the active layer based on different substrates. From the figure we can figure out that the surface thickness of the film scraped out on the composite transport layer is uniform, with better morphology, which hasn't a wide range of height differences.

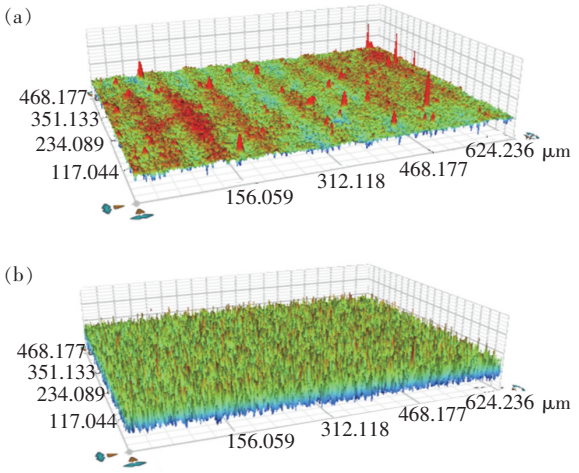

Fig. 8 Three-dimensional surface morphology of active layer based on glass substrate/AZO/active layer(a) and glass substrate/AZO/BPhen/active layer(b) structure

Fig. 9 and Tab. 1 show the film thickness values in different regions. By measuring the film thickness of the active layer film in different areas, we found that when the new composite transport layer was used as the substrate, the uniformity of the film thickness of the active layer improved greatly. This improvement is very important for enhancing the performance of the module device, which indicates that the performance of each battery in the series battery module prepared is equivalent, thereby ensuring the overall device performance.

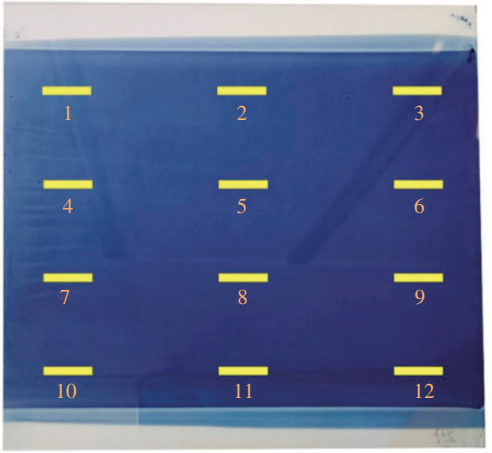

Fig. 9 Film locations of different areas

Tab. 1　Thickness of different areas of the active layer based on different substrates

	Point	Thickness/nm
AZO/Active layer	1	135
	2	113
	3	102
	4	126
	5	165
	6	135
	7	142
	8	102
	9	113
	10	151
	11	147
	12	105
AZO/BPhen/Active layer	1	120
	2	115
	3	126
	4	110
	5	118
	6	121
	7	112
	8	128
	9	108
	10	131
	11	125
	12	116

3.3　Photovoltaic Characteristics of Organic Solar Cell Modules Based on Different Transport Layers

Based on two different transport layer substrates, we prepared the traditional organic solar cell module devices ITO/AZO/PM6∶Y6/MoO_3/Al and new composite transport layer ITO/AZO/Bphen/PM6∶Y6/MoO_3/Al organic solar cell module devices. Fig. 10 shows the density *versus* voltage (*J-V*) curves of OSCs with BPhen of different thicknesses. The electron dense layer (BPhen) with 10 nm thicknesses is the most optimized device, which demonstrated a high photoelectric conversion efficiency (PCE) of 10.62%. The main effect of BPhen's thickness is the electron transmission capacity for devices performance. If the BPhen's thickness is too thick, the electron transmission capacity becomes weak. If it is too thin, which will not form an electron dense layer.

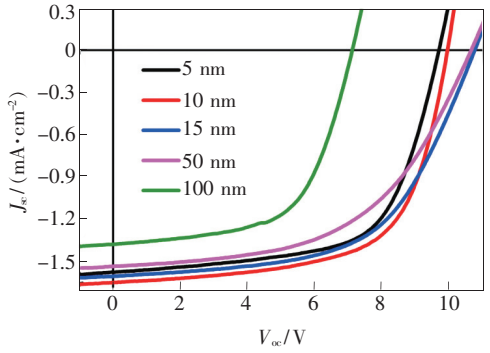

Fig. 10　*J-V* curves of OSCs with BPhen of different thicknesses

From the *J-V* and external quantum efficiency (EQE) curves of the rigid organic solar cell module devices with different structures as shown in Fig. 11(a) and the photovoltaic parameters in Tab. 2, we can found that when the composite transport layer is used, the uniformity of the morphology has a significant improvement. By improved and enhanced the carrier mobility, the device performance has been

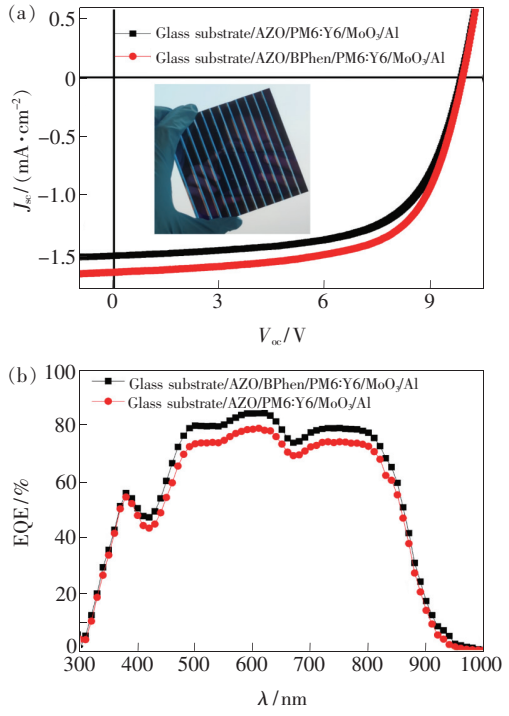

Fig. 11　(a) *J-V* curves of rigid organic solar cell modules with different structures. (b) EQE curves of rigid organic solar cell modules with different structures.

greatly improved, which mainly manifested by the increase in short-circuit current density J_{sc} and fill factor FF, J_{sc} increased from 1.51 mA/cm^2 to 1.65 mA/cm^2, FF from 63.04% to 64.15%. It shows that the film formed based on the new type of transport layer substrate has better film formation properties, fewer defects inside, and higher conversion efficiency of the absorbed photons. The PCE of the final prepared new rigid module device was improved to 10.62%, about an increase of 13%. As shown in Fig. 11(b), the EQE of the device(from 450 to 800 nm) shows a slight improvement owing to the morphological optimization of blend films. Furthermore, 82% of EQE is obtained in the device with BPhen, exhibiting much stronger ability to collect carriers.

Tab. 2 Photovoltaic performance of rigid organic solar cell modules with different structures

Rigid modules	V_{oc}/V	J_{sc}/(mA · cm^{-2})	FF/%	PCE/%	Active area/cm^2
Traditional	9.88	1.51	63.04	9.40	36
New composite	9.92	1.65	64.15	10.62	36

Fig. 12 shows the evolution of the PCE of cells under AM1.5(100 mW/cm^2 air mass 1.5 illumination). The performance of the reference cells degrades slowly. After 168 h, the PCE of the cells decreases from 10.62% (V_{oc} = 9.92 V, J_{sc} = 1.65 mA/cm^2, and FF = 63.04%) to 9.26% (V_{oc} = 9.62 V, J_{sc} = 1.50 mA/cm^2, and FF = 62.4%), and the PCE of traditional cell decreases from 9.40%(V_{oc} = 9.88 V, J_{sc} = 1.51 mA/cm^2, and FF = 63.04%) to 5.23% (V_{oc} = 9.02 V, J_{sc} = 1.08 mA/cm^2, and FF = 53.68%). J_{sc} and FF of the large area devices are decreased, but new composite large-area modular devices show good stability.

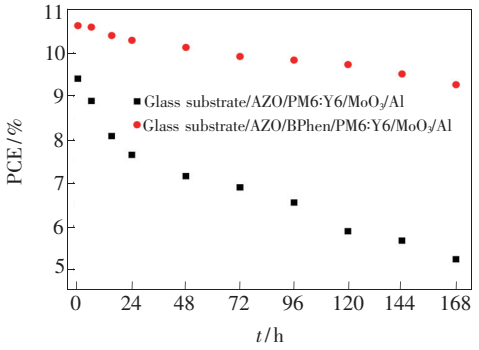

Fig. 12 Evolution of the PCE of cells under AM1.5(100 mW/cm^2 air mass 1.5 illumination)

From the *J-V* curve of flexible organic solar cell module devices with different structures as shown in Fig. 13 and the photovoltaic parameters in Tab. 3, it can be seen that the new composite transport layer also has a good device performance on the flexible substrate. Compared with traditional module devices, the photovoltaic parameters have been greatly improved. V_{oc} increased from 8.59 V to 9.01 V, J_{sc} increased from 1.10 mA/cm^2 to 1.26 mA/ cm^2 and FF increased from 41.11% to 44.78%. In the end, the photoelectric conversion efficiency of its flexible module devices reached 5.13%, about an increase of 32%. Finally, it shows that adding an electronic dense layer on the surface of the rough PET substrate can effectively increase the surface

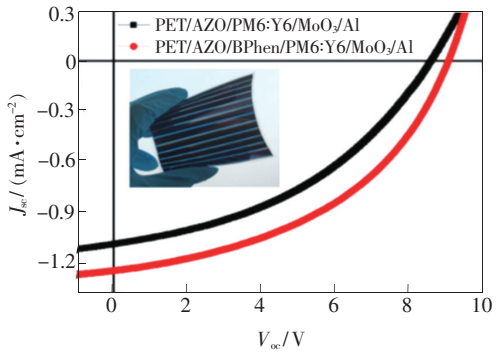

Fig. 13 *J-V* curves of flexible organic solar cell modules with different structures

Tab. 3 Photovoltaic performance of flexible organic solar cell modules with different structures

Flexible modules	V_{oc}/V	J_{sc}/(mA · cm^{-2})	FF/%	PCE/%	Active area/cm^2
Traditional	8.59	1.10	41.11	3.89	36
New composite	9.06	1.26	44.78	5.13	36

flatness, which has great application potential in the improvement of the performance of flexible module devices in the future.

4 Conclusion

In this study, a new type of composite transport layer is constructed by introducing an electron dense layer into the traditional transport layer. The combination of blade coating and evaporation techniques not only improved the optical and electrical properties of the film, but also reduced the roughness of the substrate and increased the substrate wettability. It is helpful for the film to form the active layer during the knife coating process, so that the film thickness is uniform and the morphology is structured. Finally, the overall photoelectric conversion efficiency of the rigid module device was greatly improved, and the PCE was increased from 9.4% to 10.62%. Moreover, it has a very good performance improvement effect on the flexible substrate, and the photoelectric conversion efficiency of the flexible module device has reached 5.13%, about an increase of 32% comparing to reference device. This research has a marked impact on the promotion of the industrialization of organic photovoltaic.

References:

[1] FUKUDA K, YU K, SOMEYA T. The future of flexible organic solar cells [J]. *Adv. Energy Mater.*, 2020, 10(25): 2000765.

[2] ZHAO F W, WANG C R, ZHAN X W. Morphology control in organic solar cells [J]. *Adv. Energy Mater.*, 2018, 8(28): 1703147.

[3] LIU D Y, WANG J Y, GU C Y, *et al.*. Stirring up acceptor phase and controlling morphology *via* choosing appropriate rigid aryl rings as lever arms in symmetry-breaking benzodithiophene for high-performance fullerene and fullerene-free polymer solar cells [J]. *Adv. Mater.*, 2018, 30(8): 1705870.

[4] GAO K, DENG W Y, XIAO L G, *et al.*. New insight of molecular interaction, crystallization and phase separation in higher performance small molecular solar cells *via* solvent vapor annealing [J]. *Nano Energy*, 2016, 30: 639-648.

[5] OSTROVERKHOVA O. Organic optoelectronic materials: mechanisms and applications [J]. *Chem. Rev.*, 2016, 116(22): 13279-13412.

[6] CHEN J D, LI Y Q, ZHU J S, *et al.*. Polymer solar cells with 90% external quantum efficiency featuring an ideal light-and charge-manipulation layer [J]. *Adv. Mater.*, 2018, 30(13): 1706083-1-8.

[7] CUI M Q, LI D, DU X Y, *et al.*. A cost-effective, aqueous-solution-processed cathode interlayer based on organosilica nanodots for highly efficient and stable organic solar cells [J]. *Adv. Mater.*, 2020, 32(38): 2002973-1-8.

[8] SONG J L, LI C, ZHU L, *et al.*. Ternary organic solar cells with efficiency >16.5% based on two compatible nonfullerene acceptors [J]. *Adv. Mater.*, 2019, 31(52): 1905645.

[9] JIANG K, WEI Q Y, LAI J Y L, *et al.*. Alkyl chain tuning of small molecule acceptors for efficient organic solar cells [J]. *Joule*, 2019, 3(12): 3020-3033.

[10] CUI Y, YAO H F, ZHANG J Q, *et al.*. Over 16% efficiency organic photovoltaic cells enabled by a chlorinated acceptor with increased open-circuit voltages [J]. *Nat. Commun.*, 2019, 10(1): 2515-1-8.

[11] LI K, WU Y S, TANG Y B, *et al.*. Ternary blended fullerene-free polymer solar cells with 16.5% efficiency enabled with a higher-LUMO-level acceptor to improve film morphology [J]. *Adv. Energy Mater.*, 2019, 9(33): 1901728.

[12] PAN M A, LAU T K, TANG Y B, *et al.*. 16.7%-efficiency ternary blended organic photovoltaic cells with PCBM as the acceptor additive to increase the open-circuit voltage and phase purity [J]. *J. Mater. Chem.* A, 2019, 7(36): 20713-20722.

[13] SUN H L, LIU T, YU J W, *et al.*. A monothiophene unit incorporating both fluoro and ester substitution enabling high-performance donor polymers for non-fullerene solar cells with 16.4% efficiency [J]. *Energy Environ. Sci.*, 2019, 12(11): 3328-3337.

[14] WANG D, QIN R, ZHOU G Q, *et al.*. High-performance semitransparent organic solar cells with excellent infrared reflection and see-through functions [J]. *Adv. Mater.*, 2020, 32(32): 2001621-1-8.

[15] WANG Y F,JIA B Y,WANG J,*et al.*. High-efficiency perovskite quantum dot hybrid nonfullerene organic solar cells with near-zero driving force [J]. *Adv. Mater.*, 2020,32(29):2002066.

[16] CHEN H Z,ZHAN L L,LI S X,*et al.*. Over 17% efficiency ternary organic solar cells enabled by two non-fullerene acceptors working in an alloy-like model [J]. *Energy Environ. Sci.*, 2020,13(2):635-645.

[17] WANG T,SUN R,SHI M M,*et al.*. Solution-processed polymer solar cells with over 17% efficiency enabled by an iridium complexation approach [J]. *Adv. Energy Mater.*, 2020,10(22):2000590.

[18] ZHANG L,XU X B,LIN B J,*et al.*. Achieving balanced crystallinity of donor and acceptor by combining blade-coating and ternary strategies in organic solar cells [J]. *Adv. Mater.*, 2018,30(51):1805041.

[19] OH S,SONG C E,LEE T,*et al.*. Enhanced efficiency and stability of PTB7-Th-based multi-non-fullerene solar cells enabled by the coexisting working mechanism of the alloy-like and energy transfer model [J]. *J. Mater. Chem.* A, 2019,7(38):22044-22053.

[20] ZHAO W C,ZHANG S Q,ZHANG Y,*et al.*. Environmentally friendly solvent-processed organic solar cells that are highly efficient and adaptable for the blade-coating method [J]. *Adv. Mater.*, 2018,30(4):1704837-1-7.

[21] LEE J,SEO Y H,KWON S N,*et al.*. Slot-die and roll-to-roll processed single junction organic photovoltaic cells with the highest efficiency [J]. *Adv. Energy Mater.*, 2019,9(36):1901805.

[22] WANG G D,ADIL M A,ZHANG J Q,*et al.*. Large-area organic solar cells:material requirements,modular designs,and printing methods [J]. *Adv. Mater.*, 2019,31(45):1805089.

[23] DONG S,JIA T,ZHANG K,*et al.*. Single-component non-halogen solvent-processed high-performance organic solar cell module with efficiency over 14% [J]. *Joule*, 2020,4(9):2004-2016.

[24] HUANG K M,WONG Y Q,LIN M C,*et al.*. Highly efficient and stable organic solar cell modules processed by blade coating with 5.6% module efficiency and active area of 216 cm^2 [J]. *Prog. Photovolt. Res. Appl.*, 2019,27(3):264-274.

[25] JI G Q,ZHAO W C,WEI J F,*et al.*. 12.88% efficiency in doctor-blade coated organic solar cells through optimizing the surface morphology of a ZnO cathode buffer layer [J]. *J. Mater. Chem.* A, 2019,7(1):212-220.

[26] YE L,XIONG Y,YAO H F,*et al.*. High performance organic solar cells processed by blade coating in air from a benign food additive solution [J]. *Chem. Mater.*, 2016,28(20):7451-7458.

[27] CHEN J D,CUI C H,LI Y Q,*et al.*. Single-junction polymer solar cells exceeding 10% power conversion efficiency [J]. *Adv. Mater.*, 2015,27(6):1035-1041.

[28] TSAI P T,YU K C,CHANG C J,*et al.*. Large-area organic solar cells by accelerated blade coating [J]. *Org. Electron.*, 2015,22:166-172.

[29] TAN L C,WANG Y L,ZHANG J W,*et al.*. Highly efficient flexible polymer solar cells with robust mechanical stability [J]. *Adv. Sci.*, 2019,6(7):1801180-1-8.

丁磊(1985 -),男,陕西咸阳人,博士,副教授,硕士研究生导师,2015年于苏州大学获得博士学位,2017年在苏州大学从事博士后研究,主要从事 OPV 和钙钛矿电池、OLED照明、OLED 微型显示器的研究。

E-mail: dinglei@ sust. edu. cn